JOURNAL OF MATERIALS SCIENCE 33 (1998) 4543–4549

# Scanning electron acoustic microscopy for the evaluation of domain structures in $BaTiO_3$ single crystal and ceramics

X. X. LIU, L. J. BALK
*Lehrstuhl für Elektronik, FB 13, Bergische Universität Gesamthochschule Wuppertal, Germany*

B. Y. ZHANG, Q. R. YIN
*Laboratory of Functional Inorganic Materials, Shanghai Institute of Ceramics, Chinese Academy of Science, People's Republic of China*
*E-mail: xxliu@uni-wuppertal.de*

As a non-destructive and subsurface detecting technique, the scanning electron acoustic microscopy (SEAM) method has been applied to study the ferrodomain structures in ferroelectric $BaTiO_3$ single crystal and ceramics. The domain arrangements and the orientations of domain walls at different geometry structures in the $BaTiO_3$ single crystal, and the relationships of domain structures with surface grains in the $BaTiO_3$ ceramics, have been discussed by analysing the experimental results obtained at different operation conditions. The distributions of electron acoustic signals with modulation frequencies up to 1 MHz have been obtained. The relationship of the electron acoustic signal with incident electron energy has also been studied. Although the thermal wave coupling mechanism makes a certain contribution to the acoustic signal generations, the image contrast of ferrodomains is dominated by differences in the electrical properties of ferroelectric materials. 

## 1. Introduction

Scanning electron acoustic microscopy (SEAM) has been widely applied in the characterization of various materials since it was first developed [1–3]. Owing to its ability for non-destructive subsurface imaging and special imaging mechanisms which are based on electrical, thermal and elastic properties of a sample and which differ from those of other electron microscopes, it has been used to study subsurface defects and doping information in semiconductor materials and devices [4, 5], martensite structures in alloy [6], and residual stress field distributions in structure ceramics [7]. Recently, it has been newly applied to observe and analyse the domain structures in ferroelectric materials [8, 9]. Because it does not need any pre-treatment of a sample surface, and a secondary electron image (SEI) of the sample topography and an electron acoustic image (EAI) can be obtained at the same time *in situ*, the SEAM method is very useful in the study of domain structures and relationships with surface features in ferroelectric materials.

Ferroelectric materials have received much attention and been used in and more applications, especially in recent years, due to their thin films which have promising uses in various microelectronic and photoelectric technologies [9]. The occurrence of spontaneous polarization and the formation of ferroelectric domains in ferroelectric materials are the basis for their applications. To study the domain structures of ferroelectric materials, numerous methods have been developed, which include optical microscopy [10], surface etching [11], powder decoration [12], scanning [13] and transmission [14] electron microscopy. These methods suffer from polishing, etching, thinning, decorating, and particularly for TEM, difficulties of sample preparation. With the establishment of SEAM, it may be possible to overcome the inconveniences mentioned above and to visualize subsurface domain structures.

In this work, SEAM has been used to study the domain structures in barium titanate single crystals, and ceramics. The electron acoustic images of domain structures in single crystals and ceramics at different experimental conditions have been obtained. The relationships between domain structures and surface features of the sample, have been analysed. The origins of electron acoustic image contrasts of the domains are preliminarily discussed. The experimental results show that the SEAM method is one of the most powerful tools available to characterize the domain structures, and provides more information which is complementary to other methods.

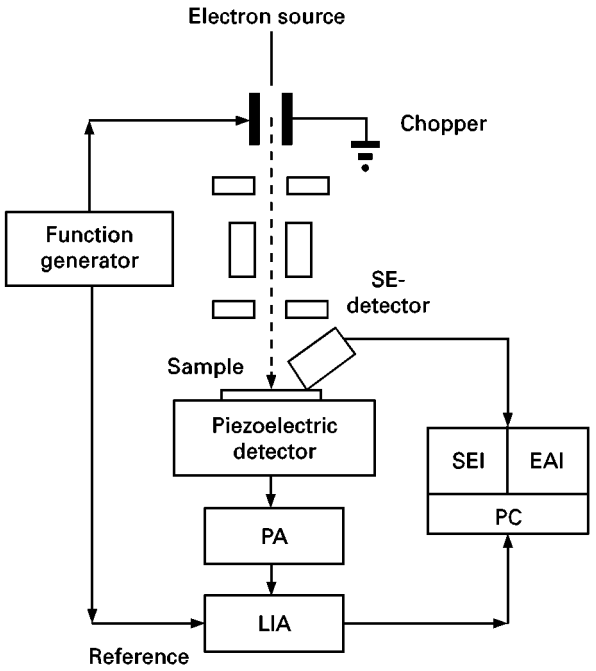


*Figure 1* Schematic diagram of the SEAM experimental set-up.

## 2. Experimental procedure

The SEAM experimental set-up is depicted in Fig. 1 and is modified from commercially used SEM. The electron beam in the SEM is modulated at a certain frequency in order to generate an acoustic wave in a sample. The electron acoustic signal is received by a piezoelectric detector which is in intimate contact with the rear surface of the sample. A pre-amplifier (PA) and a lock-in amplifier (LIA) are used to process the signal. Both the SE and EAI obtained *in situ* can be shown simultaneously on the screen of a computer.

The samples used in the experiment were barium titanate single crystals and ceramics. $BaTiO_3$ material belongs to the perovskite structure, whose Curie temperature is about 120 °C. When it passes its ferroelectric phase transition temperature (Curie temperature), its space group changes from cubic $m3m$ to tetragonal 4 mm. The orientation of spontaneous polarization, $P_s$, can be along any of three crystal axes because of the equivalence in the cubic phase. So, there are only adjacent 90° and 180° spontaneously polarized regions in the $BaTiO_3$ material, which are often called 90°-domains and 180°-domains.

## 3. Results and discussion

### 3.1. SEAM of $BaTiO_3$ single crystal

The sample of $BaTiO_3$ single crystal in the experiment was about 0.5 mm thick and the *a*-axis of the sample was perpendicular to the observed surface. The domain structures in the centre have been investigated. Fig. 2 shows the experimental results observed in the middle of the sample.

Fig. 2a shows the SEI which gives only the surface topography features. Fig. 2b–d are EAIs obtained at different modulation frequencies at the same position. Neat arrangements of domain structures with alternate black and white strips, occur in the electron acoustic images. The widths of the domains are uniform in all of the picture and have average values of 8 μm. In addition, the defects on the surface (for example, arrow C in Fig. 2c) and in the subsurface (arrow D in Fig. 2c) of the sample are also revealed in the EAI. By comparing Fig. 2b, c and d, more information about the surface defects of the sample can be observed with the increase of the modulation frequency.

However, the acoustic signal of domain structures does not change, in principle, with modulation frequencies. Fig. 3 shows the acoustic signals of domain structures in a linescan. The line scan position is the same for three different modulation frequencies, as illustrated as AB line in Fig. 2b. The profiles basically exhibit no changes due to the uniformity of thermal properties and the domain structures in the bulk of the observed single crystal. Not further details concerning the domain structures can be found with increasing modulation frequency, as shown in Fig. 3.

Fig. 4 shows the domain wall distribution on two different planes. The samples has two surfaces: one plane (abcd) with optical flatness, the other plane (cdef) with a cleavage plane (Fig. 4e). Fig. 4a shows the SEI of the two planes. Because the SEI is only a two-dimensional image, the boundary line (line cd in Fig. 4) between the two planes is not clear in Fig. 4a. Fig. 4b shows the EAI at $f = 119.3$ kHz of the sample, and the domain structures and domain walls can be seen clearly. The schematic arrangements of the domain structures and the possible orientations of domain walls are shown in Fig. 4f. The same sample has been thinned 30 μm along the plane abcd, by direct grinding and an EAI at $f = 198.1$ kHz (Fig. 4c) has been achieved. It can be seen that domain structures on the newly formed plane abcd are destroyed and the domain structures on the plane cdef, to which nothing has been done, are also changed. Fig. 4d is the EAI at $f = 169.1$ kHz of the same sample, which has been thinned a further 24 μm, in the same way for the second time. It can be seen that all the regular distributions of domain structures on both planes have totally vanished. This phenomenon could be explained by the assumption that the changes in the internal energy of the ferroelectric material can influence the domain structures. When the sample in thinned along the plane abcd for the first time (Fig. 4c), the domain structures on this plane are changed. Furthermore, the thinning also has some influence on the domains in the plane cdef and the domain structures on this plane are also changed. When the sample is thinned a further 24 μm, along the plane abcd for the second time, the internal energy of the sample is changed so greatly that the regular domain structures on both surfaces vanish. We can also see that the crystal has a break in the middle of the sample (as illustrated by arrows in Fig. 4d).

### 3.2. SEAM of $BaTiO_3$ ceramics

The observed $BaTiO_3$ ceramics sample was made by in standard sintering technique and the thickness of the sample was about 1.0 mm. The surface of the

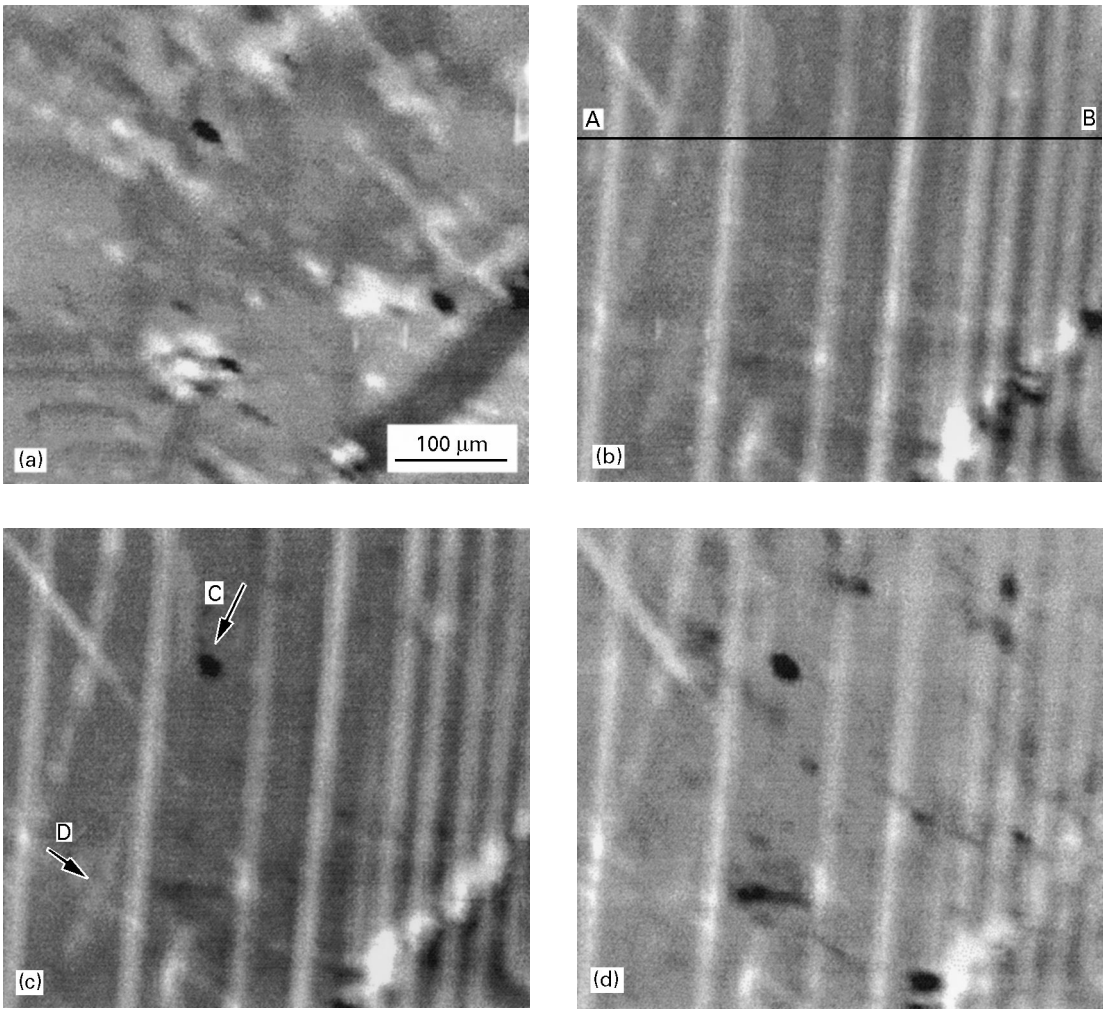


*Figure 2* (a) SEI, and EAI at (b) $f = 38.3$ kHz, (c) $f = 84.5$ kHz and (d) $f = 182.8$ kHz of $BaTiO_3$ single crystal.

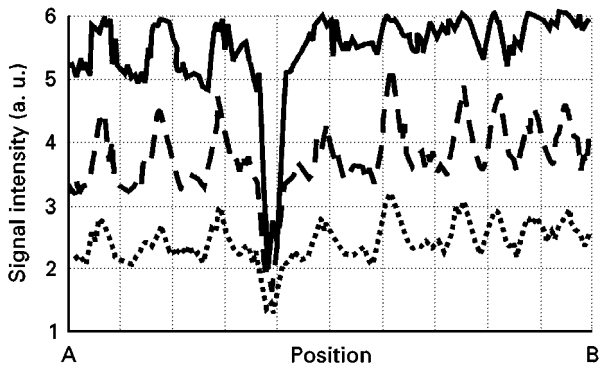


*Figure 3* Dependence of the lateral resolution of the electron acoustic signal on the modulation frequency in SEAM of $BaTiO_3$ single crystal. $f$ : (- - -) 38.3 kHz, ( — — — ) 84.5 kHz, (—) 182.2 kHz.

sample was only coated with a gold film. Many well-grown grains (see Fig. 5a as illustrated by the arrows) have domain structures which can be clearly observed in Fig. 5b. A typical photograph of the domain structure relationship with surface grains, taken by SEAM, is given in Fig. 5. By comparison of Fig. 5a and b, it can be seen that one kind of orientation of domain arrangements can cross several grains and multi-orientations of domain arrangements can be found in a single grain. The first phenomenon requires that the sample has a minimum energy at a stable state, and the second phenomenon implies that the grain is a "twin grain". Moreover, the domains either cross the boundary or are parallel to each other on the boundary of two neighbouring grains. Thus the observed domains are always in the surface which is a well-known fact for $BaTiO_3$. The arrangements and the widths of domains in the interior of the grains are uniform.

Fig. 6 illustrates the lateral resolution of the electron acoustic signal with respect to the modulation frequency. Two line profiles containing 200 points have been obtained at the same location at 154.2 and 208.1 khz, respectively. By comparing the two line profiles, it is revealed that there are some variations between them, which differs from the results for the single crystal. This implies that the thermal coupling mechanism affects the probing depth and resolution due to a different thermal wavelength. The non-uniformity of grains which decides the domain structures in the materials, is revealed at different modulation frequencies.

In some areas (about 50 μm) of two grain boundaries, the domains cross the boundary in the form of a "grain domain". This phenomenon implies non-uniform grain structures on the grain boundary. This effect of "grain domain" is also observed in those grains which are not well grown and have defects. Fig. 7b is an enlargement of the square outlined in

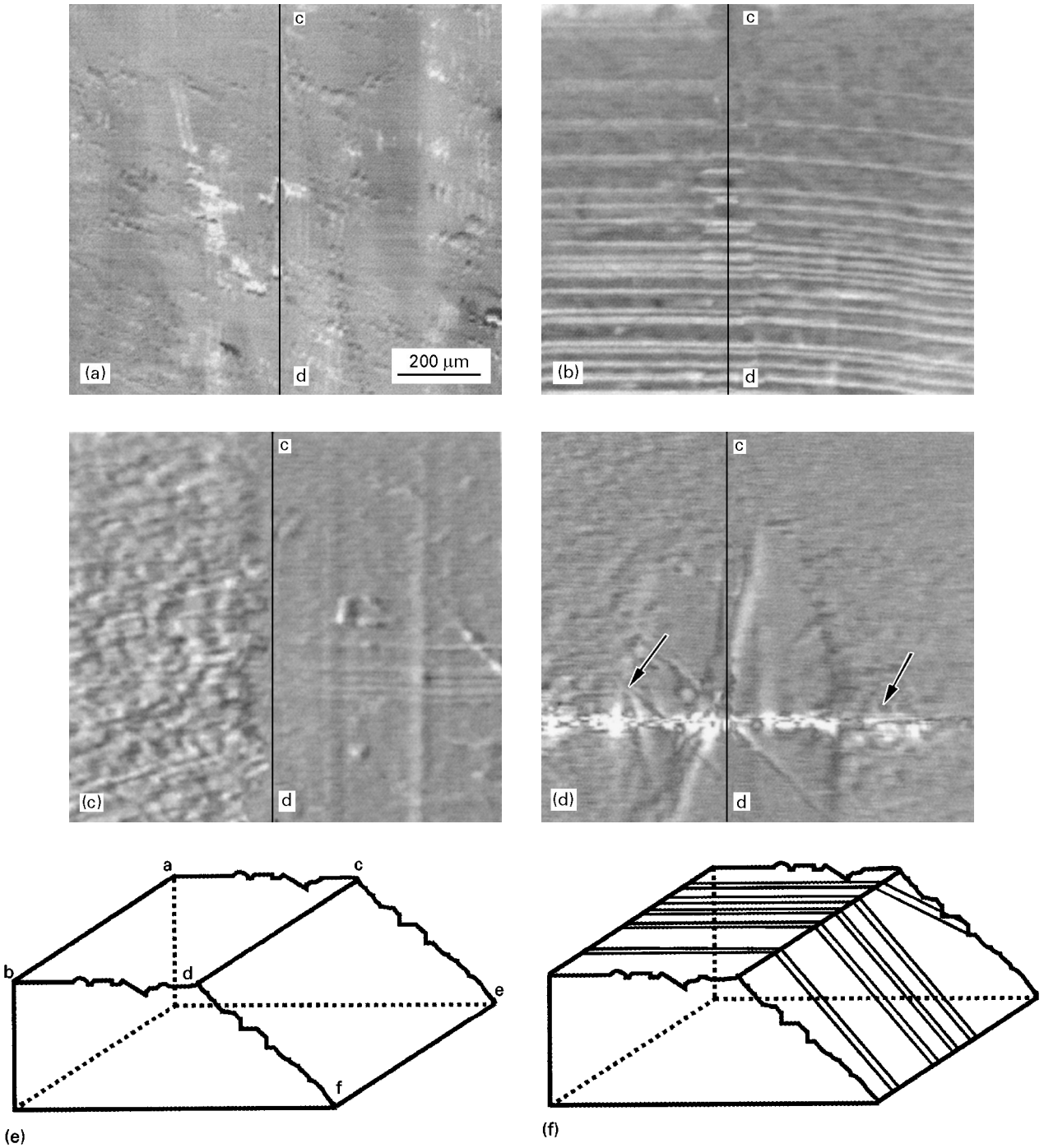


*Figure 4* (a) SEI, and EAI at (b) $f = 119.3\,\text{kHz}$, (c) $f = 198.1\,\text{kHz}$ after thinning 30 μm, (d) $f = 169.1\,\text{kHz}$ after thinning 54 μm, (e) schematically depicted cross-section, and (f) arrangements of domain structures and the possible orientations of domain walls of $BaTiO_3$ single crystal at the edge of the sample.

Fig. 7a, which shows more clearly the "grain domain" structures in the boundary of two neighbouring grains.

The relationships between the amplitude of the electron acoustic signals with the incident energy of the electron beams have also been studied. As a function of incident electron beam current, the magnitude of the SEAM signal at 20 kV accelerating voltage is shown in Fig. 8. The position of the linescan is the same for different incident energies, as the line AB indicated in Fig. 5b.

Fig. 9 shows the variation of SEAM signals with different accelerating voltages at the same incident beam current. With increasing beam current, the SEAM signal has clearly increased. The clearer pictures of domain structures and higher resolution are obtained at larger electron beam currents. Along with the alternation of accelerating voltage, the quality of EAI and the resolution have virtually not changed. These experimental results imply that the density of energy dissipation determines the magnitude of the signal in the SEAM of $BaTiO_3$ ceramics.

Fig. 10 shows the frequency dependence of the electron acoustic signal from 10–1020 kHz at a fixed scanning line. The line scanning position is the same for different modulation frequencies. Along with the variation of modulation frequency, the magnitude of the electron acoustic signal undergoes undulation.

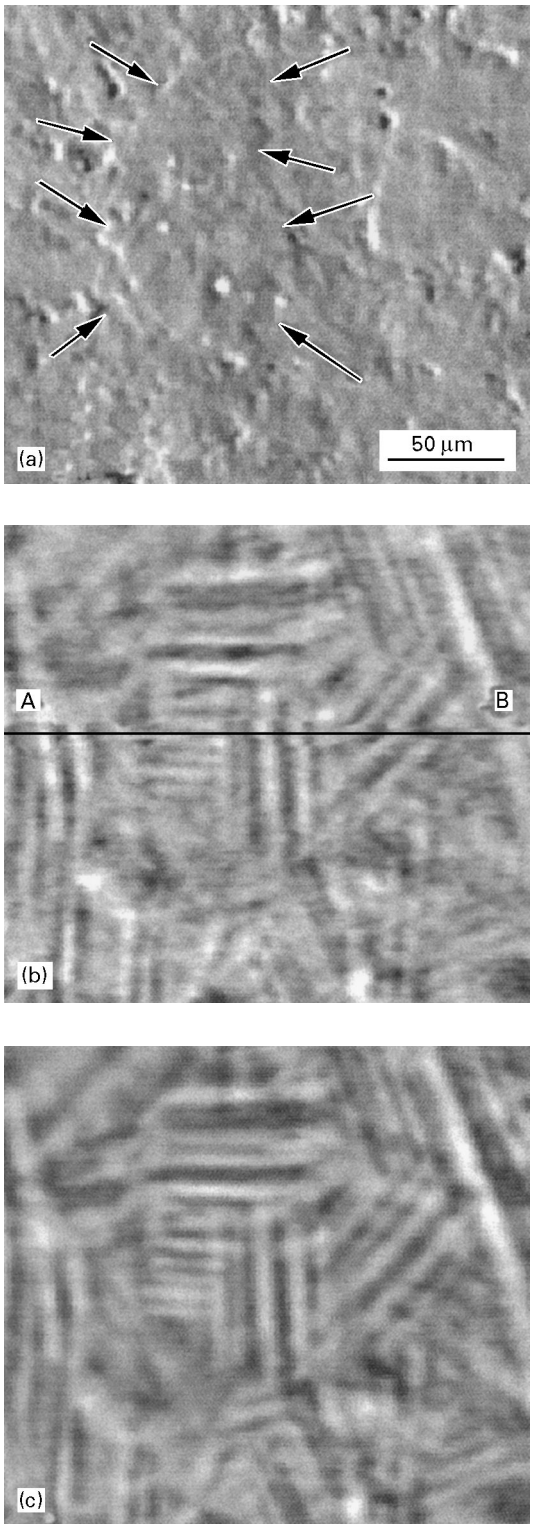


*Figure 5* (a) SEI, and EAI at (b) $f = 154.2$ kHz and (c) $f = 208.1$ kHz of $BaTi_3$ ceramics.

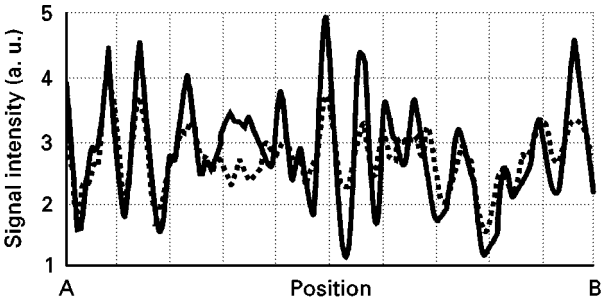


*Figure 6* Dependence of the lateral resolution of the electron acoustic signal on the modulation frequency in the SEAM of $BaTiO_3$ ceramics; the scanning line position is indicated in Fig. 5b. $f$ : (- - -) 154.2 kHz, (—) 208.1 kHz.

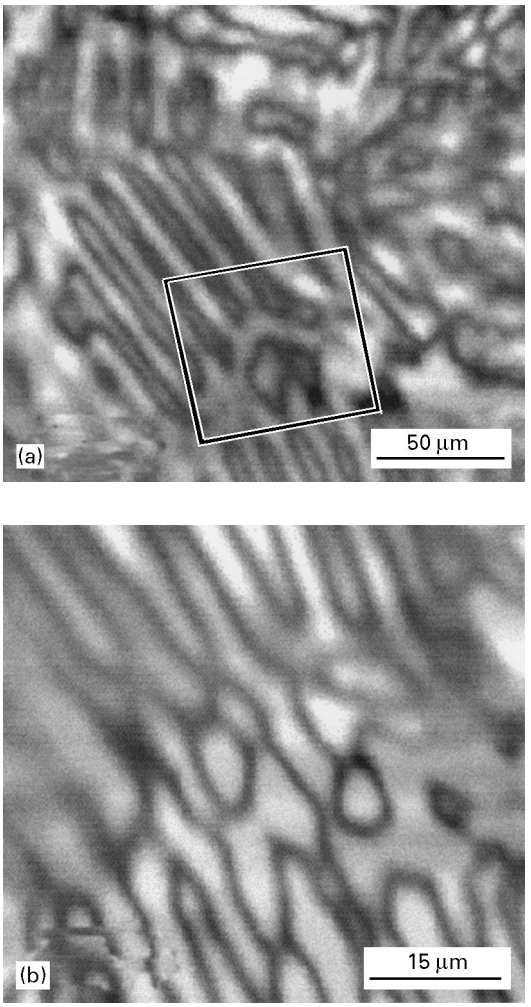


*Figure 7* EAI of a "grain domain" in $BaTiO_3$ ceramics; EAI at (a) $f = 206.8$ kHz and (b) $f = 186.1$ kHz; (b) is an enlargement of the square outlined in (a).

The ranges of the relatively stronger electron acoustic signal are mainly in the areas of 10–600 kHz. This may be related to the distribution of the frequency response curve of the transducer used.

## 3.3. Discussion of electron acoustic image contrasts

Many papers have been devoted to the electron acoustic signal generation mechanisms [16–20]. However, comprehensive and mature theory of electron acoustic imaging mechanisms has not yet been given because various factors (electrical, thermal and elastic) make simultaneous contributions to the acoustic signal generation. It is difficult to vary one of the material parameters without changing another. A detail review of several possible acoustic signal generation mechanisms in SEAM is given elsewhere [20].

It is well known that when an electron beam is directed into the sample, a thermal wave will always be generated due to the difference in thermal properties of the sample. It could be deduced that the thermal

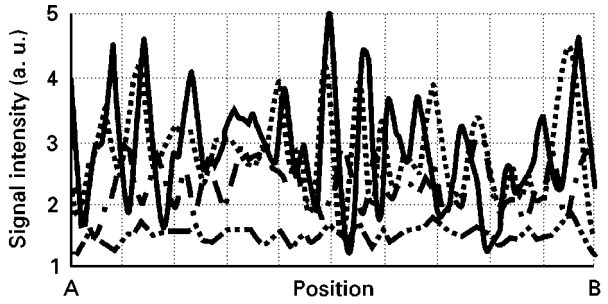


*Figure 8* Dependence of the amplitude of the electron acoustic signal on the incident electron beam current at 20 kV accelerating voltage. ( — - - — ) 2.2 mW, ( — - — ) 5.2 mW, (- - -) 8.0 mW, (—) 13.4 mW.

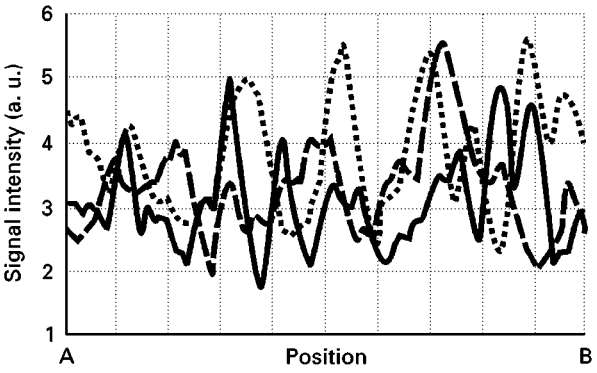


*Figure 9* Dependence of the amplitude of the electron acoustic signal on the accelerating voltage at the same electron beam current. (—) 20 kV, (- - -) 18 kV, ( — — — ) 16 kV.

wave coupling mechanism will play a certain role in the electron acoustic signal generations in the SEAM of $BaTiO_3$ materials. By comparing Fig. 2b, c and d, more information about features, such as defects on the surface and in the subsurface, etc., can be found at high modulation frequency. This is because of the decrease of detecting depth with increase of the modulation frequency, according to the thermal wave coupling mechanism. Moreover, the domain structures in Fig. 2b–d show no changes with increasing modulation frequency. This implies that the image contrast of domain structures in SEAM would not be due to the thermal wave coupling mechanism. The differences in the electrical properties among the domain structures in the sample, such as spontaneous polarization, dielectric nature and electric conductivity, would be

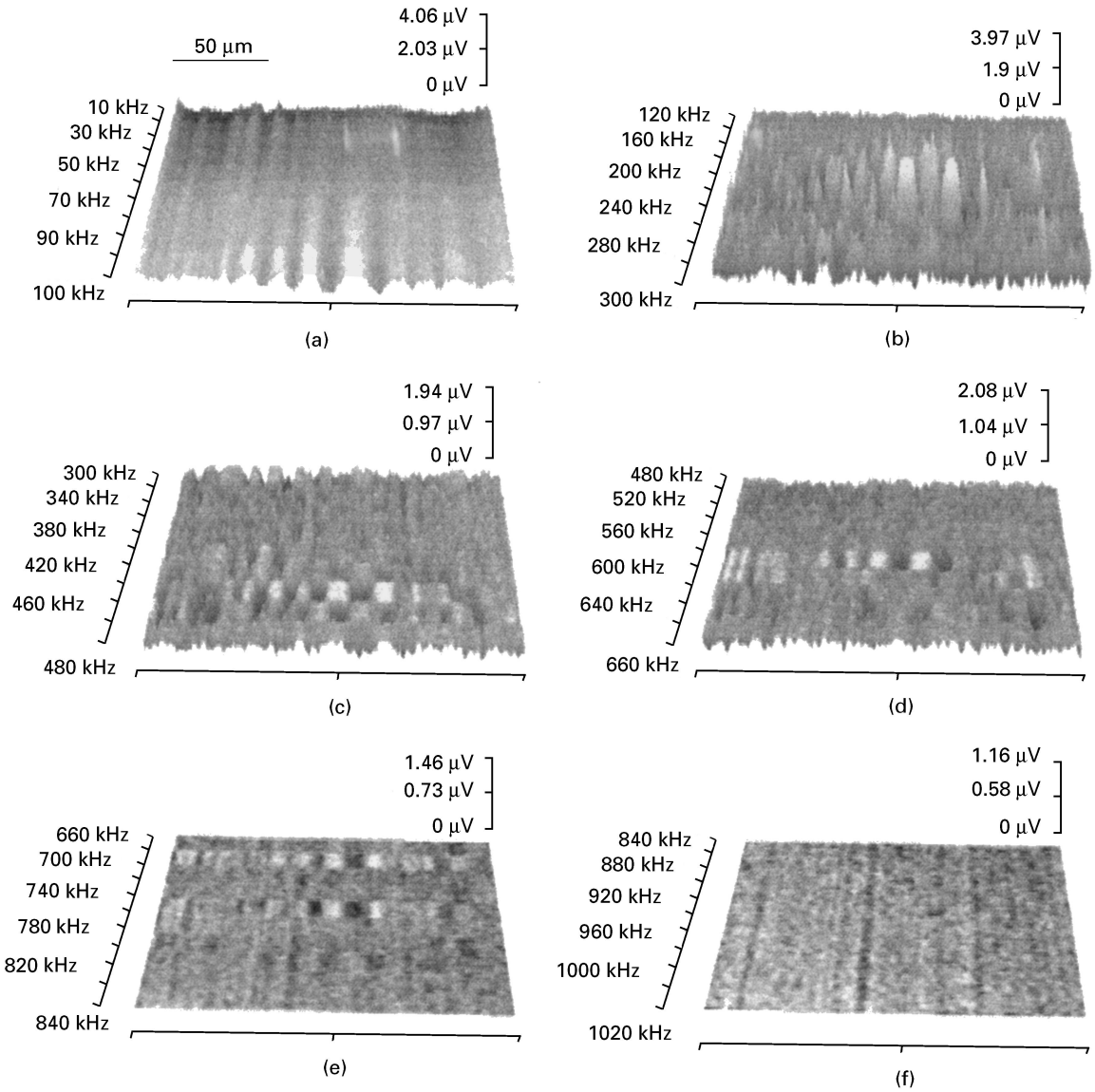


*Figure 10* Frequency dependence of the electron acoustic signal in SEAM of $BaTiO_3$ ceramics.

dominant over the origins of image contrasts of the domains. The same conclusion can be deduced by analysing the profiles of the dependence of the electron acoustic signal on the modulation frequency in Fig. 3. According to the thermal wave coupling mechanism, the resolution, $\delta$, is directly proportional$^{/2}$ and more detailed information about the domain structures should be given with the increase of modulation frequency. No evidence of this phenomenon can be found by comparing Figs. 3 and Fig. 2b–d.

In the same way, we can deduce that the different electrical properties (spontaneous polarization, dielectric nature and electric conductivity) among the domain structures in the $BaTiO_3$ ceramics are also related to the origins of the electron acoustic image contrasts of the domains. However, from Fig. 5b and c it can be seen that the image contrasts between the domain structures in ceramics have relatively greater variations than those in single crystals. This is because the uniformity of composition in the ceramic materials of $BaTiO_3$ is worse than that in $BaTiO_3$ single crystals. The changes in thermal properties in ceramics are greater than those in single crystals. Moreover the domain structures exhibit variations at different depths in the ceramic sample. Thus, the variations of electron acoustic image contrasts in the ceramics are comparatively distinct from those in single crystals, together with the changes of modulation frequency.

From the above discussion, we can deduce that the thermal wave coupling mechanism plays only a certain role in the acoustic signal in SEAM. When an electron beam is directed into the sample, the energy of the electron beam will be partially absorbed by the sample. The absorbed energy will affect the interior electric field and set up a new electric field in the sample. Because of the piezoelectric properties of the sample, an acoustic wave will be directly generated in the sample. Therefore, the origins of image contrasts of domain structures will be decided by the difference in the electrical properties in the $BaTiO_3$ single crystal and ceramics. In addition, non-linear electron acoustic images in the SEAM of $BaTiO_3$ materials could not be obtained.

## 4. Conclusion

The usefulness and the abilities of SEAM for studying and visualizing domain structures at different geometrical conditions in ferroelectric materials, have been shown. The observation of domain structures is possible without pre-treatment of the sample surface, and the sample is not destroyed. Because both the electron acoustic image of domain structures and the secondary electron image of the sample surface topography can be obtained at the same time *in situ*, SEAM can provide more information about the relationships between surface features and domain structures. The origins of the electron acoustic image contrasts of domains have been preliminary discussed owing to the complicated signal generation mechanisms in the SEAM of ferroelectric materials. In addition, domain structures may be visualized in real time in SEAM, therefore, the study of the influence of different parameters on ferroelectric domains and the observation of phase transitions of ferroelectric will be possible in future. The study of static and dynamic domain properties by the SEAM method is in progress.


## Acknowledgements

The authors thank Dr R. Heiderhoff for helpful discussions and R. E. Stephan for the experimental help and discussions. Dr Luo Haosu and Dr Xue Jiming, Shanghai Institute of Ceramics, are thanked for supplying the barium titanate samples.


## References


1. G. S. CARGILL III, *Nature* **286** (1980) 691.
2. E. BRANDIS and A. ROSENCWAIG, *Appl. Phys. Lett.* **37** (1) (1980) 98.
3. L. J. BALK and N. KULTSCHER, *Inst. Phys. Conf. Ser.* **67** (1983) 387.
4. L. J. BALK and N. KULTSCHER, in "*Scanning Electron Microscopy Conference*", 17–22 April 1983, Dearborn, USA.
5. H. TAKENOSHITA, *Solar Cells* **16** (1986) 65.
6. L. J. BALK, D. G. DAVIES and N. KULTSCHER, *Phys. Status Solidi* (*a*) **82** (1984) 23.
7. B. Y. ZHANG, F. M. JIANG, Y. SHI, M. L. QIAN and Q. R. YIN, *Appl. Phys. Lett.* **70** (1997) 589.
8. B. Y. ZHANG, F. M. JIANG, Y. Y. YANG, Q. R. YIN and S. KOJIMA, *J. Appl. Phys.* **80** (1996) 1901.
9. B. Y. ZHANG, X. X. LIU, M. MAYWALD, Q. R. YIN and L. J. BALK, in "*The* 23rd *International Symposium on Acoustic Imaging*", 13–16, April 1997, Boston, USA.
10. C. P. DE ARAUJO, J. F. SCOTT and G. W. TAYLOR (eds), "Ferroelectric Thin Films: Synthesis and Basic Properties", (Gordon and Breach, The Netherlands, 1996).
11. V. P. KONSTANTINOVA, N. A. TICHOMIROVA and M. GLOGAROVA, *Ferroelectrics* **20** (1978) 259.
12. J. A. HOOTON and W. J. MERZ, *Phys. Rev.* **98** (1955) 409.
13. G. L. PEARSON and W. L. FELDMANN, *J. Phys. Chem. Solids* **9** (1958) 28.
14. R. LEBIHAN and M. MAUSSION, *J. Phys.* **33** (1972) 2.
15. PENG JU LIN and L. A. BURSILL, *Philos. Mag.* A48 (1983) 25.
16. M. E. LINES and A. M. GLASS, "Principle and Applications of Ferroelectrics and Related Materials", (Clarendon Press, Oxford, 1977) pp. 89–90.
17. J. OPSAL and A. ROSENCWAIG, *J. Appl. Phys.* **53** (1982) 4240.
18. N. KULTSCHER and L. J. BALK, *J. Scanning Electron Microsc.* **I** (1986) 33.
19. L. J. BALK, D. G. DAVIES and N. KULTSCHER, *IEEE Trans. Magn.* **MAG-20** (1984) 1466.
20. B. Y. ZHANG and Q. R. YIN, in "*Proceedings of the* 9th *International Conference on photoacoustic and photothermal phenmenona*", 27–30 June 1996, Nanjing, China, pp. S123–6.
21. L. J. BALK, "Scanning Electron Acoustic Microscopy", in "Advances in Electronics and Electron physics", vol. **71** (Academic Press, Boston, MA, 1988) pp. 1–74.



*Received 24 December 1997*
*and accepted 15 May 1998*